Transport in Porous Media (2022) 143:47–68
https://doi.org/10.1007/s11242-022-01784-6

A Fully Coupled Hydro-Mechanical-Gas Model Based on Mixture Coupling Theory

Sulaiman Abdullah[1] · Yue Ma[1] · Xiaohui Chen[1] · Amirul Khan[1]

Received: 29 August 2021 / Accepted: 11 April 2022 / Published online: 14 May 2022

Abstract

The interactions of gas migration, water transport and mechanical deformation of rocks are significant for geoenergy industry (e.g. Carbon Capture and Storage, radioactive waste disposal); however, the hydro-mechanical-gas coupled model remains a challenge due to the gap between multiple disciplines (e.g. Geomechanics and Geoenergy). This work presents a novel hydro-mechanical framework model of fully coupled two-phase fluid transport in a deformable porous media through extending mixture coupling theory which is based on non-equilibrium thermodynamics. The main difference between the mixture coupling theory approach and other approaches (ex., mechanic's approach) is that the mixture coupling theory uses energy and entropy analysis by utilizing the unbalanced thermodynamics, while the mechanic's approach analyses the stress–strain tensors. The gas free energy has been included in the Helmholtz free energy balance equation. Three main governing equations have been obtained for solid, liquid and gas phases. Benchmark experiments and modelling based on classical continuum mechanics approaches are used to validate the model by comparing the measured data to the simulation results. The results have a good agreement with experimental data, demonstrating that gas migration has a great influence on water transport and deformation of the solids. The novelty of this study is that it is providing a new approach to study the multiphase flow coupling in porous media rather than the classic mechanic's approach.

Article Highlights

- **A Hydro-Mechanical-Gas (HMG) model has been developed using the mixture coupling theory approach.**
- **The hydro-mechanical framework equations were established by using non-equilibrium thermodynamic and Darcy law.**
- **The model has been validated using published experimental data and the results of other researchers with different approaches.**

Keywords Biot's theory · Non-equilibrium thermodynamics · Mixture coupling theory · Two-phase fluid transport · Unsaturated

✉ Xiaohui Chen
x.chen@leeds.ac.uk

[1] School of Civil Engineering, University of Leeds, Leeds LS2 9JT, UK

List of Symbols

$\mathbf{d}$	Displacement tensor
C_s	Specific moisture capacity
$\mathbf{E}$	Green strain
E_{ij}	Green Strain tensor
$\mathbf{F}$	Deformation gradient
G	The rock's shear modulus
$\mathbf{I}$	Unit tensor
J	Jacobian
k	Bulk modulus
k_{abs}	Medium Intrinsic permeability
K_s	Bulk modulus of the solid matrix
K_w	Bulk modulus of water
K_g	Bulk modulus of gas.
k_w	Water intrinsic permeability
k_g	Gas intrinsic permeability
k_{rw}	Water relative permeability
k_{rg}	Gas relative permeability
p^w	Pore water pressure
p^g	Pore gas pressure
$\overline{p}$	Average pressure in pore space
S	Boundary attached on the surface
S^w	Saturation of water
S^g	Saturation of gas
T	Temperature
T_{ij}	Piola–Kirchhoff stress
t	Time
$\mathbf{u}w$	Darcy velocity of pore water
$\mathbf{u}^g$	Darcy velocity of pore gas
V	Arbitrary microscopic domain
$\mathbf{v}^{\text{w}}$	Water velocity
$\mathbf{v}^g$	Gas velocity
$\mathbf{v}^s$	Solid velocity
ν^w	Water viscosity
ν^g	Gas viscosity
ρ^w	Water density relative to the unit volume of the fluid–solid mixture
ρ^g	Gas density relative to the unit volume of the fluid–solid mixture
ρ^s	Solid density relative to the unit volume of the fluid–solid mixture
ρ_t^w	Water true mass density
ρ_t^g	Gas true mass density
ϕ^w	Water volume fraction
ϕ^g	Gas volume fraction
ϕ	Porosity
ψ	Helmholtz free energy density
ψ_{pore}	Helmholtz free energy density of the pore Constituent
Ψ	Free energy in the reference configuration
$\boldsymbol{\sigma}$	Cauchy stress tensor
μ^w	Chemical potential of water
μ^g	Chemical potential of gas

ε_{ij}	Strain tensor
σ_{ij}	Cauchy stress
γ	Entropy production per unit volume
υ^w	Volume fraction of pore water in the reference configuration
υ^g	Volume fraction of pore gas in the reference configuration
ζ	Biot's coefficient
θ	Poisson's ratio
∇	Gradient
∂	Partial differential

1 Introduction

Over the past years, fluid transport in porous media has become an area of great interest for researchers. It is now considered an essential part of studies in the oil industries and environmental institutes. However, modelling the transport of fluids in porous media is complicated due to the coupled nature of the phenomena and the corresponding governing equations with large number of variables. Many approaches have been developed to capture the transportation process. Moreover, coupling between solid and fluid phases can be modelled using two main approaches: the mechanics approach and the mixture coupling theory approach based on the mixture theory. The mechanics approach is based on a classical consolidation theory described by (Biot 1941, 1955, 1962; Biot and Temple 1972) and extended from the derivation of stress–strain balance equations. Biot created a coupled relation between fluid flow and linear elasticity for solid deformation (poroelasticity), which was used to calculate the deformation in the porous media.

On the other hand, the mixture theory approach, developed by Truesdell (1957), Truesdell and Toupin (1960), is based on the derivation of the energy balance equation of non-equilibrium thermodynamics using continuum mechanics. Bowen (1980), Bowen (1982) used the mixture theory to model incompressible fluids in porous media. The approach maintains the individuality of the solid and fluid phases and takes into account the phase interaction effects. Heidug and Wong (1996) present the first coupled model based on the mixture theory that capture hydration swelling of water-absorbing saturated rocks under isothermal condition.

Chen and Hicks (2011) used the mixture coupling theory to model the hydro-mechanical effect in unsaturated rock. Their model is a result of combining the non-equilibrium thermodynamics and Biot's poroelasticity. They built their model by deriving Darcy's law for unsaturated flow from the dissipation process and establishing a relationship between stress and pore pressure changes using Helmholtz free energy. Chen and Hicks proposed that their model is capable of capturing both small and large deformation of rocks.

Nowadays, the mixture theory approach is widely used in various fields, including the biomechanics field, where it is used to model the biological interstitial tissue growth, solid tumours and blood flow (Please et al. 1998, Klika 2014; Cardoso et al. 2013). The mixture theory is also used in the oil field and earth sciences to model carbon capture and storage, reservoir modelling and enhancing oil recovery. Furthermore, the mixture theory method is used in the environmental field to study nuclear waste disposal and groundwater contamination, and in construction studies, to analyse asphalt concrete (Siddique et al. 2017; Krishnan and Rao 2000).

The mixture coupling theory can deal with molecular scale effects, and this gives it a great potential to couple chemical reactions process with the hydro-mechanical calculations. As a result, mixture coupling theory can bridge the gap between the geomechanics and geochemistry field.

The mixture coupling theory may be used to couple multi-equations together, such as the poroelasticity process (HM), the thermo-poroelasticity process (THM), the poroelasticity-chemical reactions process (HMC) or all together as (THMC).

In soil mechanics, gas migration in the unsaturated formation, such as soil and rocks, is crucial. The big difference in viscosity, density and compressibility between the gas phase and liquid phase cause a significant coupled impact on the hydro-mechanical part. Additionally, gases such as carbon dioxide or other organic gases may have a considerable chemical impact. In real applications, such as enhancing hydrocarbon production or carbon injection and storage, gas migration needs to be considered. Therefore, including gas migration in the mathematical model is a vital step. The existing mechanics approach can handle coupled hydro-mechanics–chemical–thermal interaction. However, the chemical coupling can be complicated and has many limitations when the mechanics approach is used. Schrefler and Scotta (2001) used the mechanics approach to establish three coupled equations that describe the mechanical behaviour, hydraulic behaviour of the water and the hydraulic behaviour of the air. The equations were then solved numerically using the finite element method. The model was validated by simulating an experiment of semi-saturated soil behaviour, triaxial load experiment with clay specimen and other two examples. However, solving such a problem using the mixture coupling theory is a step forward.

In this work, anew model is presented based on the mixture coupling theory approach. The model will be used to capture and evaluate the hydro-mechanical effect of gas and water flow in porous media.

2 Physical Model

An arbitrary microscopic domain V, which is large enough to include all types of phases, is selected. S is the surface boundary enclosing the domain V. Only fluids (e.g. water or gas) are allowed to pass through the boundary.

2.1 Definition of Flux, Density, Volume Fraction and Saturation

The mass flux of water and gas is defined as

$$\mathbf{I}^w = \rho^w(\mathbf{v}^w - \mathbf{v}^s),\ \mathbf{I}^g = \rho^g(\mathbf{v}^g - \mathbf{v}^s) \tag{1}$$

where the superscripts w, g and s denote water, gas and solid, respectively. ρ^w,ρ^g are the mixture density of water and gas, related to the volume of the mixture system. $\mathbf{v}^w$, $\mathbf{v}^g$ and $\mathbf{v}^s$ is the velocity of each phase.

ρ^w, ρ^g are related to the true mass density (associated with the volume of phases) of water ρ_t^w and gas ρ_t^g through:

$$\rho^w = \phi^w \rho_t^w,\ \rho^g = \phi^g \rho_t^g \tag{2}$$

where ϕ^w and ϕ^g are the volume fraction of water and gas.

$$\phi = \phi^w + \phi^g \tag{3}$$

ϕ is the porosity.

The saturation of water and gas is:

$$S^w = \frac{\phi^w}{\phi}, \; S^g = \frac{\phi^g}{\phi} \tag{4}$$

Clearly, there is a relationship:

$$S^g = 1 - S^w \tag{5}$$

2.2 Balance equation

The balance equation for Helmholtz free energy in a mixture system including solid, water and gas is:

$$\frac{D}{Dt}\int_V \psi dV = \int_S \boldsymbol{\sigma}\mathbf{n} \cdot \mathbf{v}^s dS - \int_S \mu^w \mathbf{I}^w \cdot \mathbf{n} dS - \int_S \mu^g \mathbf{I}^g \cdot \mathbf{n} dS - T\int_V \gamma dV \tag{6}$$

where ψ is Helmholtz free energy density, $\boldsymbol{\sigma}$ is the Cauchy stress tensor, μ^w is the chemical potential of water, μ^g is the chemical potential of gas, T is temperature, γ is the entropy production per unit volume. Equation (6) is an extension of the Helmholtz free energy balance equation under constant temperature presented by Heidug and Wong (1996), by adding the gas flux to represent the free energy change due to gas flowing into/out the selected domain.

The material time derivative is

$$\frac{D}{Dt} = \partial_t + \mathbf{v}^s \cdot \nabla \tag{7}$$

in which ∂_t is the time derivative and ∇ the spatial gradient.

The differential form of the balance Eq. (6) for the free energy is expressed as

$$\dot{\psi} + \psi \nabla \cdot \mathbf{v}^s - \nabla \cdot (\boldsymbol{\sigma}\mathbf{v}^s) + \nabla \cdot (\mu^w \mathbf{I}^w) + \nabla \cdot (\mu^g \mathbf{I}^g) = -T\gamma \leq 0 \tag{8}$$

Balance equation for water mass is

$$\frac{D}{Dt}\left(\int_V \rho^w dV\right) = -\int_S \mathbf{I}^w \cdot \mathbf{n} dS \tag{9}$$

The differential form is

$$\dot{\rho}^w + \rho^w \nabla \cdot \mathbf{v}^s + \nabla \cdot \mathbf{I}^w = 0 \tag{10}$$

Balance equation for gas mass is

$$\frac{D}{Dt}\left(\int_V \rho^g dV\right) = -\int_S \mathbf{I}^g \cdot \mathbf{n} dS \tag{11}$$

The differential form is

$$\dot{\rho}^g + \rho^g \nabla \cdot \mathbf{v}^s + \nabla \cdot \mathbf{I}^g = 0 \tag{12}$$

2.3 Entropy Product and Transport Law

The entropy product arises from the dissipative processes, namely, the friction generated at the solid/fluid phase boundary when the fluid moves through a solid matrix. The entropy product can be divided into two parts: entropy induced by water fraction and gas fraction. By using non-equilibrium thermodynamics, the entropy production is described by Katachalsky and Curran (1965) as:

$$-\mathbf{I}^w \cdot \nabla \mu^w - \mathbf{I}^g \cdot \nabla \mu^g = T\gamma \geq 0 \tag{13}$$

The Darcy velocity of pore water $\mathbf{u}^w$ and gas $\mathbf{u}^g$ is:

$$\mathbf{u}^w = S^w \phi (\mathbf{v}^w - \mathbf{v}^s) \tag{14}$$

$$\mathbf{u}^g = S^g \phi (\mathbf{v}^g - \mathbf{v}^s) \tag{15}$$

Then, based on the entropy product $T\gamma^w = -\mathbf{I}^w \cdot \nabla \mu^w$ and $T\gamma^g = -\mathbf{I}^g \cdot \nabla \mu^g$, the Darcy's Law for water and gas transport can be obtained through using Phenomenological Equations (Chen and Hicks 2011):

$$\mathbf{u}_w = -k_w \frac{k_{rw}}{\nu^w} \nabla p^w \tag{16}$$

$$\mathbf{u}_g = -k_g \frac{k_{rg}}{\nu^g} \nabla p^g \tag{17}$$

where k_w, k_g are the intrinsic permeability for water and gas, k_{rw} and k_{rg} are the relative permeability, ν^w and ν^g are the viscosity, p^w and p^g are the pore water pressure and pore gas pressure.

2.4 Hydro-mechanical Framework Equation

2.4.1 Basic Equation for Deformation

The soil/rock is assumed to be in mechanical equilibrium, so that $\nabla \cdot \boldsymbol{\sigma} = \mathbf{0}$. With the entropy production (13) and balance Eq. (8), the equation for ψ can be written as:

$$\dot{\psi} + \psi \boldsymbol{\nabla}.\mathbf{v}^s - (\sigma : \boldsymbol{\nabla} \mathbf{v}^s) + \mu^w \boldsymbol{\nabla} \cdot \mathbf{I}^w + \mu^g \boldsymbol{\nabla} \cdot \mathbf{I}^g = 0 \tag{18}$$

The classic continuum mechanics is used here to measure the rock's deformation state. Some basic relationships are needed: for an arbitrary reference configuration $\mathbf{X}$, with time denoted by t and position by $\mathbf{x}$, the expression of Green strain $\mathbf{E}$, and deformation gradient $\mathbf{F}$ are expressed as:

$$\mathbf{F} = \frac{\partial \mathbf{x}}{\partial \mathbf{X}}(\mathbf{X}, t),\ \mathbf{E} = \frac{1}{2}\left(\mathbf{F}^{\mathbf{T}}\mathbf{F} - \mathbf{I}\right) \tag{19}$$

where $\mathbf{I}$ is a unit tensor.

The second Piola–Kirchhoff stress $\mathbf{T}$ is introduced to measure the stress in the reference configuration, and it is related to the Cauchy stress $\boldsymbol{\sigma}$ by:

$$\mathbf{T} = J\mathbf{F}^{-1}\boldsymbol{\sigma}\mathbf{F}^{-T} \tag{20}$$

where J is the Jacobian of $\mathbf{F}$:

$$J = \frac{dV}{dV_0},\ \dot{J} = J\nabla\mathbf{v}^s \tag{21}$$

dV is the volume in the current configuration and dV_0 is the volume in the reference configuration.

From Eqs. (10), (12), and (18), with Eqs. (19), (20), and (21), it leads to:

$$\dot{\Psi} = tr(\mathbf{T}\dot{\mathbf{E}}) + \mu^w \dot{m}^w + \mu^g \dot{m}^g \tag{22}$$

in which: $\Psi = J\psi$ is the free energy in the reference configuration, $m^\beta = J\rho^\beta = JS^\beta \phi \rho_t^\beta$ is the mass density of the pore water ($\beta = w$)/gas($\beta = g$) in the reference configuration.

2.4.2 Helmholtz Free Energy Density of Pore Water/Gas

The Helmholtz free energy density of the pore constituent, including water and gas, is denoted as ψ_{pore}. Then, based on classical thermodynamics, the free energy density of pore space can be written as:

$$\psi_{\text{pore}} = -\overline{p} + S^w \rho_t^w \mu^w + S^g \rho_t^g \mu^g \tag{23}$$

where $\overline{p}$ is the average pressure in pore space and is described as:

$$\overline{p} = p^w S^w + p^g S^g \tag{24}$$

By substituting Eq. (24) into Eq. (23), $\overline{p}$ can be eliminated as:

$$\dot{\psi}_{\text{pore}} = -(p^w S^w) - (p^g S^g)^{\cdot} + \dot{\mu}^w \left(S^w \rho_t^w\right) + \mu^w \left(S^w \rho_t^w\right)^{\cdot} + \dot{\mu}^g \left(S^g \rho_t^g\right) + \mu^g \left(S^g \rho_t^g\right)^{\cdot} \tag{25}$$

Applying Gibbs–Duhem equation in a constant temperature to pore water and gas separately, it leads to:

$$\begin{aligned} S^w \dot{p}^w &= \dot{\mu}^w S^w \rho_t^w \\ S^g \dot{p}^g &= \dot{\mu}^g S^g \rho_t^g \end{aligned} \tag{26}$$

and then, with Eqs. (25) and (26), it leads to

$$\dot{\psi}_{\text{pore}} = -p^w \dot{S}^w - p^g \dot{S}^g + \mu^w \left(S^w \rho_t^w\right)^{\cdot} + \mu^g \left(S^g \rho_t^g\right)^{\cdot} \tag{27}$$

2.4.3 Free Energy Density of the Wetted Mineral Matrix

The free energy density of the wetted matrix can be obtained by subtracting the free energy of pore water/gas from the total free energy of the combined rock/water/gas system.

From Eqs. (22) and (27), the free energy of the wetted mineral matrix is obtained as:

$$\left(\Psi - J\phi\psi_{\text{pore}}\right)^{\cdot} = tr\left(\mathbf{T}\dot{\mathbf{E}}\right) + \overline{p}\dot{\upsilon} \tag{28}$$

where $\upsilon = J\phi$ is the volume fraction of the pores in the reference configuration.

The dual potential can be expressed as

$$W = \left(\Psi - J\phi\psi_{pore}\right) - \overline{p}\upsilon \tag{29}$$

By substituting Eq. (28) into the time derivation of the Eq. (29), it leads to:

$$\dot{W} = tr(\mathbf{T}\dot{\mathbf{E}}) - \dot{\overline{p}}\upsilon \tag{30}$$

where W is a function of $\mathbf{E}$, and $\overline{p}$, so the expression of $\mathbf{T}$, and υ can be given**.** Equation (30) implies the time derivative of $W(\mathbf{E}, \overline{p})$ satisfies the relation:

$$\dot{W}(\mathbf{E}, \overline{p}) = tr(\mathbf{T}\dot{\mathbf{E}}) - \dot{\overline{p}}\upsilon \tag{31}$$

and then

$$T_{ij} = \left(\frac{\partial W}{\partial E_{ij}}\right)_{\overline{p}}, \ \upsilon = -\left(\frac{\partial W}{\partial \overline{p}}\right)_{E_{ij}} \tag{32}$$

and

$$\dot{W}(\mathbf{E}, \overline{p}) = \left(\frac{\partial W}{\partial E_{ij}}\right)_{\overline{p}} \dot{E} + \left(\frac{\partial W}{\partial p}\right)_{E_{ij}} \dot{\overline{p}} \tag{33}$$

$$\dot{T}_{ij} = L_{ijkl}\dot{E}_{kl} - M_{ij}\dot{\overline{p}} \tag{34}$$

$$\dot{\upsilon} = M_{ij}\dot{E}_{ij} + Q\dot{\overline{p}} \tag{35}$$

where the parameters L_{ijkl},M_{ij},Q are as following group equations

$$\begin{aligned} L_{ijkl} &= \left(\frac{\partial T_{ij}}{\partial E_{kl}}\right)_{\overline{p}} = \left(\frac{\partial T_{kl}}{\partial E_{ij}}\right)_{\overline{p}} \\ M_{ij} &= -\left(\frac{\partial T_{ij}}{\partial \overline{p}}\right)_{E_{ij}} = \left(\frac{\partial \upsilon}{\partial E_{ij}}\right)_{E_{ij}} \\ Q &= \left(\frac{\partial \upsilon}{\partial \overline{p}}\right)_{E_{ij}} \end{aligned} \tag{36}$$

2.5 Coupled Hydro-mechanical Governing Equations

2.5.1 Mechanical Behaviour

Equations (34), (35) provided the general coupled equation for the mechanical behaviour, water pressure, gas pressure, large deformation, and anisotropic condition. This

article focuses on the coupling of mechanical water and gas, so some assumptions are made to simplify the discussion:

(i) The mechanical behaviour is regarded to be a small strain condition, so the Green Strain tensor E_{ij} and Piola–Kirchhoff stress T_{ij} can be replaced by strain tensor ε_{ij} and Cauchy stress σ_{ij}.

$$E_{ij} \approx \varepsilon_{ij}, \quad T_{ij} \approx \sigma_{ij} \tag{37}$$

(ii) The parameters L_{ijkl},M_{ij},Q are material-dependent constants, and the material is isotropic. Therefore, the tensor M_{ij} is diagonal and can be written in the forms of scalars ζ as

$$M_{ij} = \zeta \delta_{ij} \tag{38}$$

(iii) To avoid mathematical complexity, in this model, the porous media is assumed to has a completely isotropic behaviour (isotropic material).

Based on the assumption (ii), the elastic stiffness L_{ijkl} can be a fourth-order isotropic tensor as

$$L_{ijkl} = G(\delta_{ik}\delta_{jl} + \delta_{il}\delta_{jk}) + (K - \frac{2G}{3})\delta_{ij}\delta_{kl} \tag{39}$$

here, G denotes the rock's shear modulus and K denotes the bulk modulus.

With Eqs. (38), (39) and (37), the governing stress Eq. (34) can be simplified to

$$\dot{\sigma}_{ij} = \left(K - \frac{2G}{3}\right)\dot{\varepsilon}_{kk}\delta_{ij} + 2G\dot{\varepsilon}_{ij} - \dot{\overline{p}}\delta_{ij} \tag{40}$$

the incremental relationship between stress and pore fluid pressure is:

$$\dot{\sigma}_{ij} = -\dot{\overline{p}}\delta_{ij} \tag{41}$$

where $\overline{p}$ is the average pressure in the pore space, and

$$\overline{p} = p^w S^w + p^g S^g = p^w S^w + p^g - S^w p^g \tag{42}$$

strain rate is related to the average pore pressure by

$$\dot{\varepsilon}_{ij} = -\frac{\dot{\overline{p}}}{3K_s}\delta_{ij} \tag{43}$$

where K_s is the bulk modulus of the solid matrix.

And volume change is related to pore fluid pressure by:

$$\dot{\upsilon} = -\phi\frac{\dot{\overline{p}}}{K_s} \tag{44}$$

Substituting Eqs. (41) and (43) into Eq. (40):

$$-\dot{\bar{p}}\delta_{ij} = \left(K - \frac{2G}{3}\right)\left(-\frac{\dot{\bar{p}}}{K_s}\delta_{ij}\right) + 2G\left(-\frac{\dot{\bar{p}}}{3K_s}\delta_{ij}\right) - \zeta\dot{\bar{p}}\delta_{ij} \tag{45}$$

From Eq. (45), it leads to:

$$\zeta = \left(1 - \frac{K}{K_s}\right) \tag{46}$$

The quantity ζ is defined as the Biot's coefficient and is related to the bulk modulus K and K_s as described in equation (46).

From Eq. (42), the average pressure can be rewritten as:

$$\dot{\bar{p}} = \left(S^w + C_s p^c\right)\dot{p}^w + \left(S^g - C_s p^c\right)\dot{p}^g \tag{47}$$

where $C_s = \frac{\partial S^w}{\partial p^c}$ is the specific moisture capacity and can be determined from the soil water characteristic curve (SWCC) or by experiments (Van Genuchten 1980, Milly 1982, Maina and Ackerer 2017). $p^c = (p^g - p^w)$ is the capillary pressure.

Then, Eq. (40) can be written as:

$$\dot{\sigma}_{ij} = \left(K - \frac{2G}{3}\right)\dot{\varepsilon}_{kk}\delta_{ij} + 2G\dot{\varepsilon}_{ij} - \zeta\left(S^w + C_s p^c\right)\dot{p}^w\delta_{ij} - \zeta\left(S^g - C_s p^c\right)\dot{p}^g\delta_{ij} \tag{48}$$

By assuming mechanical equilibrium condition $\partial\sigma_{ij}/\partial x_j = 0$, and using displacement variables $d_i (i = 1, 2, 3)$ through $\varepsilon_{ij} = \frac{1}{2}(d_{i,j} + d_{j,i})$, it leads to

$$G\nabla^2\dot{\mathbf{d}} + \left(\frac{G}{1-2\theta}\right)\nabla(\nabla\cdot\dot{\mathbf{d}}) - \zeta\nabla\left[\left(S^w + C_s p^c\right)\dot{p}^w\right] - \zeta\nabla\left[\left(S^g - C_s p^c\right)\dot{p}^g\right] = 0 \tag{49}$$

In which θ is Poisson's ratio.

2.5.2 Fluid Phase

By substituting water density Eq. (2), and saturation Eq. (4) in to water partial mass Eq. (10):

$$\left(\rho_t^w \phi S^w\right)^{\cdot} + \rho_t^w \phi S^w \nabla\cdot\mathbf{v}^s + \nabla\cdot\left(\rho_t^w \phi S^w(\mathbf{v}^w - \mathbf{v}^s)\right) = 0 \tag{50}$$

By using Darcy velocity equation (14):

$$\left(\rho_t^w \phi S^w\right)^{\cdot} + \rho_t^w \phi S^w \nabla\cdot\mathbf{v}^s + \nabla\cdot\left(\rho_t^w \mathrm{u}^w\right) = 0 \tag{51}$$

By multiplying both side by the Jacobian J and using Euler identity as $\dot{J} = J\nabla.\mathrm{v}_s$ and $\upsilon = J\phi$, the conservation equation of water can be written as:

$$\left(S^w \upsilon \rho_t^w\right)^{\cdot} + \nabla\cdot\left(\rho_t^w \mathbf{u}^w\right) = 0 \tag{52}$$

By expanding the derivation terms:

$$S^w \dot{\upsilon}\rho_t^w + \dot{S}^w \upsilon \rho_t^w + S^w \upsilon \dot{\rho}_t^w + \nabla\cdot(\rho_t^w \mathbf{u}^w) = 0 \tag{53}$$

By using assumption (i), and Eqs. (38), (35) can be written as:

$$\dot{\upsilon} = \zeta \delta_{ij} \dot{\epsilon}_{ij} + Q\dot{\bar{p}} \tag{54}$$

The parameter Q can be obtained by eliminating $\dot{\upsilon}$, and $\dot{\epsilon}_{ij}$ by using Eqs. (43), and (44) into Eq. (54):

$$-\phi \frac{\dot{\bar{p}}}{K_s} = \zeta \delta_{ij} \left(-\frac{\dot{\bar{p}}}{K_s} \right) + Q\dot{\bar{p}} \tag{55}$$

$$Q = \frac{\zeta - \phi}{K_s} \tag{56}$$

Substituting Eq. (54), and Darcy's law for water (16) in to equation (53):

$$S^w \left(\zeta \delta_{ij} \dot{\epsilon}_{ij} + Q\dot{\bar{p}} \right) \rho_t^w + + \dot{S}^w \upsilon \rho_t^w + S^w \upsilon \dot{\rho}_t^w + \nabla \cdot \rho_t^w \left(-\mathrm{k_w} \frac{k_{rw}}{\nu^w} \nabla p^w \right) = 0 \tag{57}$$

By using displacement variables $d_i (i = 1, 2, 3)$ through $\varepsilon_{ij} = \frac{1}{2}(d_{i,j} + d_{j,i})$, Eq. (47) to eliminate the average pore pressure rate, and Q value from Eq. (56) into Eq. (57):

$$\begin{aligned} &\zeta S^w \rho_t^w \nabla \cdot \dot{\mathbf{d}} + \frac{\zeta - \phi}{K_s} S^w \rho_t^w \left(S^w + C_s p^c \right) \dot{p}^w + \frac{\zeta - \phi}{K_s} S^w \rho_t^w \left(S^g - C_s p^c \right) \dot{p}^g \\ &+ \dot{S}^w \upsilon \rho_t^w + S^w \upsilon \dot{\rho}_t^w + \rho_t^w \left(-\mathrm{k_w} \frac{k_{rw}}{\nu^w} \nabla^2 p^w \right) = 0 \end{aligned} \tag{58}$$

The water density change equation:

$$\dot{\rho}_t^w = \rho_t^w \left(\frac{1}{\rho_t^w} \frac{\partial \rho_t^w}{\partial p^w} \right) \frac{\partial p^w}{\partial t} = \rho_t^w \frac{1}{K_w} \dot{p}^w \tag{59}$$

where K_w is the bulk modulus of water.

By combining (59) with (58) leads to:

$$\begin{aligned} &\zeta S^w \rho_t^w \nabla \cdot \dot{\mathbf{d}} + \left(\frac{\zeta - \phi}{K_s} S^w \rho_t^w \left(S^w + C_s p^c \right) + \frac{S^w \phi \rho_t^w}{K_w} \right) \dot{p}^w \\ &+ \frac{\zeta - \phi}{K_s} S^w \rho_t^w \left(S^g - C_s p^c \right) \dot{p}^g + \dot{S}^w \phi \rho_t^w + \rho_t^w \left(-\mathrm{k_w} \frac{k_{rw}}{\nu^w} \nabla^2 p^w \right) = 0 \end{aligned} \tag{60}$$

Separate the C_s terms from the brackets and recall the definition of C_s, then equation (60) becomes:

$$\begin{aligned} &\zeta S^w \nabla \cdot \dot{\mathbf{d}} + \left(\frac{\zeta - \phi}{K_s} S^w S^w + \frac{S^w \phi}{K_w} \right) \dot{p}^w + \frac{\zeta - \phi}{K_s} S^w S^g \dot{p}^g \\ &+ \left(-\frac{\zeta - \phi}{K_s} S^w p^c + \phi \right) \dot{S}^w + \left(-\mathrm{k_w} \frac{k_{rw}}{\nu^w} \nabla^2 p^w \right) = 0 \end{aligned} \tag{61}$$

2.5.3 Gas Phase

With a similar derivation process to Sect. 2.4.2, the final gas governing equation can be obtained:

$$\zeta S^g \nabla \cdot \dot{\mathbf{d}} + \left(\frac{\zeta - \phi}{K_s} S^g S^g + \frac{S^g \phi}{K_g} \right) \dot{p}^g + \frac{\zeta - \phi}{K_s} S^g S^w \dot{p}^w + \left(\frac{\zeta - \phi}{K_s} S^g p^c + \phi \right) \dot{S}^g + \left(-\mathrm{k_g} \frac{k_{rg}}{v^g} \nabla^2 p^g \right) = 0 \tag{62}$$

where K_g is the bulk modulus of gas.

3 Numerical Solution

Many researchers (Schrefler and Scotta 2001; Laloui et al. 2003; Hu et al. 2011; Kim and Kim 2013; Islam et al. 2020; Wei et al. 2020) have used the drainage test performed by Liakopoulos (1965) as a benchmark test to validate numerical models for unsaturated porous media. In this work, Comsol Multiphysics software is used to simulate the drainage test to validate the proposed model. The simulation results were compared to the experimental results. However, since Liakopoulos (1965) only measured the water pore pressure and the water outflow rate of the system, the rest of the results, such as air pressure, displacement, capillary pressure and water saturation, are compared to Schrefler and Scotta (2001).

The objective of the Liakopoulos (1965) experiment is to study the fully saturation condition in a gradual desaturation state development. In the proposed experiment, 1.0 m length and 10 cm diameter perspex column was filled with Del Monte sand with top and bottom exposed to the atmospheric pressure. The walls of the tube walls are assumed to be rigid and impermeable for both water and air (no lateral displacement at the sides boundary and no flow). Tensiometers were used to measure the change of pore pressure along with column height. Only gravitational force is considered in the process. The column of sand is then constantly fed with water from the top until a constant flow rate is established through the column, and the drainage flow from the bottom through a filter becomes steady (inflow = outflow). After achieving the uniform flow condition, the water flow supply from the top is terminated (considered as time $t = 0$). The water then starts to drain due to gravity.

In this numerical simulation, the capillary pressure calculation is valid for saturation $S^w > 0.91$. The relative permeability is calculated using Brooks and Corey (1966) model as following:

$$S^w = 1 - 0.10152 \left(\frac{p^c}{\rho_w g} \right)^{2.4279}, \quad k_{\mathrm{rw}} = 1 - 2.207(1 - S^w)^{1.0121} \tag{63}$$

Table 1 shows the experiment's parameter; however, some of these properties were not provided by Liakopoulos himself, such as Young's modulus and Poisson's ratio. However, they were estimated by other researchers such as Lewis and Schrefler (1998).

For the numerical solution, assumptions have been made to conform with the laboratory conditions; first, the drainage process occurs due to gravity force only along the vertical direction. Second, at $t = 0$, the porous media is fully saturated with water ($S^w = 1$). Moreover, for the sake of simplicity, the porosity change is neglected in this simulation.

Table 1 Material parameters

Physical meaning	Values and units
Young's modulus	$E = 1.3\,\text{MPa}$
Water density	$\rho^w = 1000\,\text{kg/m}^3$
Gas density (air)	$\rho^g = 1.2\,\text{kg/m}^3$
Solid density (sand)	$\rho^s = 2000\,\text{kg/m}^3$
Poisson's ratio	$\theta = 0.2$
Biot's coefficient	$\zeta = 1$
Porosity	$\phi = 0.2975$
Intrinsic permeability of the solid (sand)	$k_{\text{abs}} = 4.5 \times 10^{-13}\ \text{m}^2$
Dynamic viscosity of water	$\nu^w = 1 \times 10^{-3}\,\text{Pa s}$
Dynamic viscosity of gas (air)	$\nu^g = 1.8 \times 10^{-5}\,\text{Pa s}$
Bulk modulus of water	$K_w = 2.0 \times 10^3\,\text{MPa}$
Bulk modulus of gas (air)	$K_g = 0.1\,\text{MPa}$
Bulk modulus of solid (sand)	$K_s = 1.0 \times 10^6\,\text{MPa}$

For the relations above, the capillary pressure should be constrained by $P^c > 0$. Moreover, to have a stable numerical solution through the transition phase from fully saturated to partially saturated state, a lower bound of 1×10^{-4} air relative permeability k_{rg} is applied. This lower bound will simulate the micro-bubbles of the air, while the system was approximating to the fully saturated state (Schrefler and Xiaoyong 1993; Hu et al. 2011).

3.1 Boundary and Initial Conditions

Liakopoulos (1965) assumed that the lateral boundary of the tube is impermeable for both water and gas. However, some researchers, such as Hu et al. (2011), suggested that the interface between the sand column and the cylinder in Liakopoulos (1965) drainage test might provide a fair passage for the air, and the experiment was not guaranteed to be a gas-tight on the lateral boundaries. Hu et al. (2011) discussed this issue and compared the two assumptions and concluded that having a gas permeable lateral boundary in the simulation gives a much better match to the experiment (outflow measurements). In this paper, the boundary condition for the air pressure at the lateral walls, the top and the bottom end of the sand column will be set as $p^g = p_{\text{atm}}$. For the initial conditions, Narasimhan (1979) mentioned that at $t = 0$, $S^w = 1$ and the pressure head was zero everywhere in the column as measured in several tensiometers distributed through the column. Because of that, the initial gas pressure and water pressure will be set as zero ($p^w = 0$, $p^g = 0$). Figure 1 shows the initial and boundary condition for the experiment simulation.

Figure 2 compares the simulation results with Liakopoulos (1965) experimental results. The figure shows the water pressure change through the vertical distance of the sand column at different time intervals (5, 10, 20, 30, 60 and 120 min). The numerical and the experimental results have a good agreement after 20 min; however, prior to this, the measured water pressure seems to decrease more slowly than the numerical solution, which dropped more rapidly. Schrefler and Scotta (2001) and many other researchers observed a similar phenomenon (Islam et al. 2020; Wei et al. 2020; Kim and Kim 2013; Gawin et al. 1997; Bandara et al. 2016) and justify it to the simplified model used for the simulation. Figure 3 through Fig. 7 compares the numerical solution with Schrefler

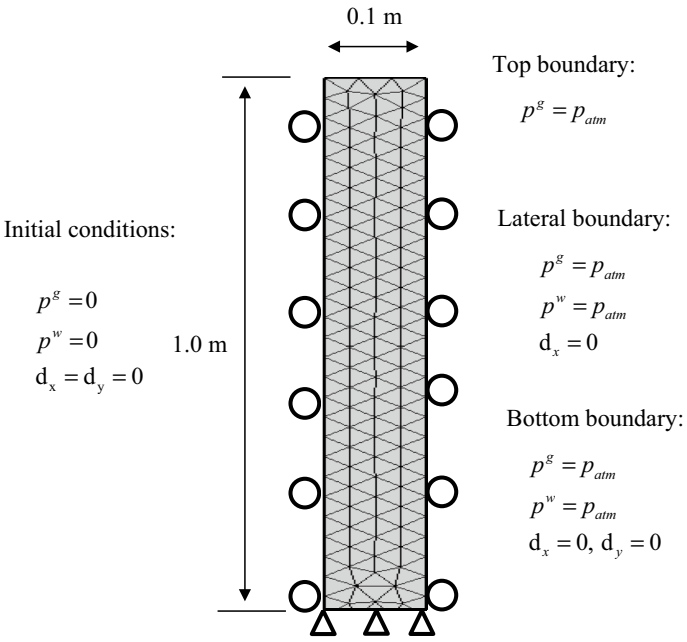

Fig. 1 Initial and boundary conditions for Liakopoulos (1965) drainage test

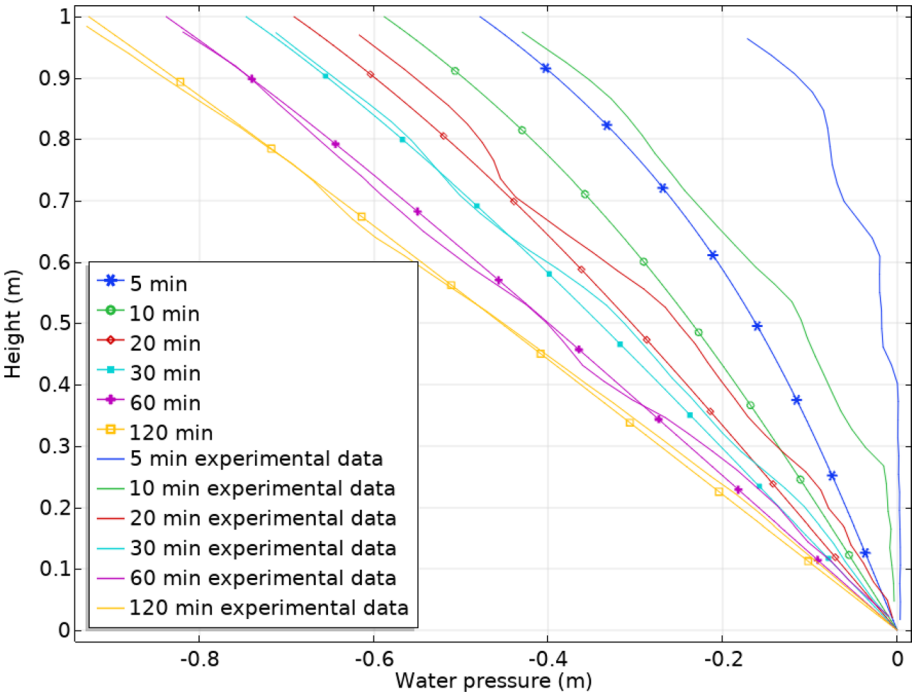

Fig. 2 Simulation results versus Liakopoulos' experiment data (water pressure)

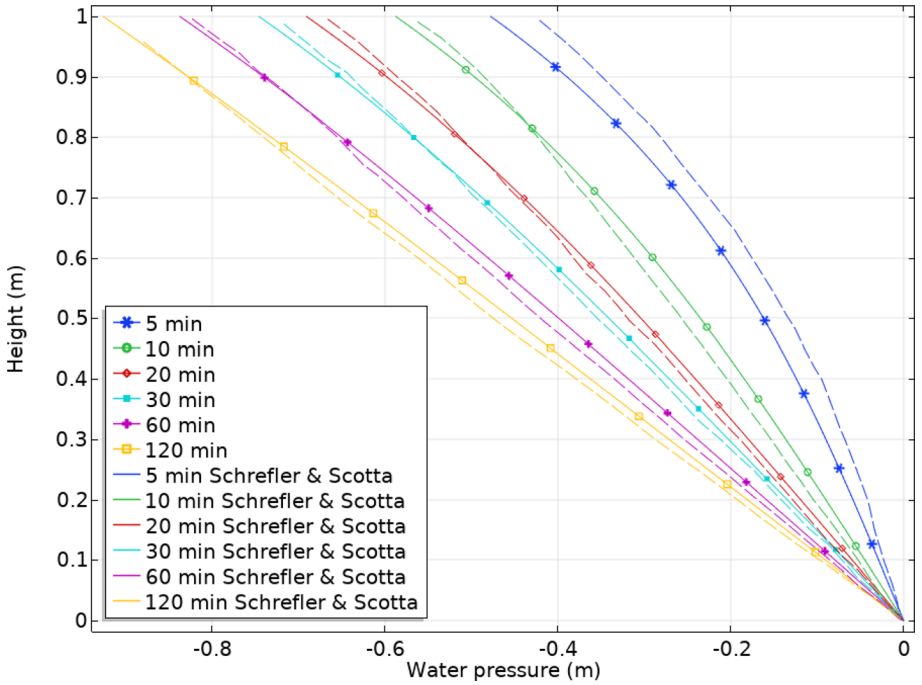

Fig. 3 Simulation results versus Schrefler and Scotta's results (water pressure)

and Scotta (2001) simulation's results. There is a clear difference in the gas (air) pressure results, as shown in Fig. 4, where the pressure peaks in Schrefler and Scotta's simulation shifted down through the column more aggressively. These differences are due to some differences in the governing equations and the numerical solution logarithm. However, Kim and Kim (2013) conducted an experiment and compared the result with Schrefler and Scotta (2001) air pressure results and found that the air pressure peaks do not move down in such a violent way. The capillary pressure in Fig. 5 is expected to be slightly different from Schrefler and Scotta's since it is directly related to the air pressure values ($p^c = p^g - p^w$). Figure 6 shows the water saturation results. The results seem close to Schrefler and Scotta's data; nonetheless, differences are justified because the water saturation calculation estimated based on Brooks and Corey (1966) model is a function of capillary pressure, as shown in Eq. (63). Finally, Schrefler and Scotta's displacement results show almost the same trend but with 36% less deformation than the mixture coupling theory model, as shown in Fig. 7. Though, when the displacement is compared to other researchers such as Islam et al. (2020), the results are almost identical (Fig. 8).

Overall, the simulation results of the proposed model have a good agreement with Liakopoulos (1965) experiment's results. The comparison between the proposed model solution and Schrefler and Scotta (2001) shows close findings with some differences that can be justified by the differences in the governing equations and the numerical approach. However, these differences are still consistent with other researchers results, as discussed earlier. As there are no reliable benchmark experimental data that shows the exact air pressure and solid-phase displacement, it is difficult to determine which model is more accurate.

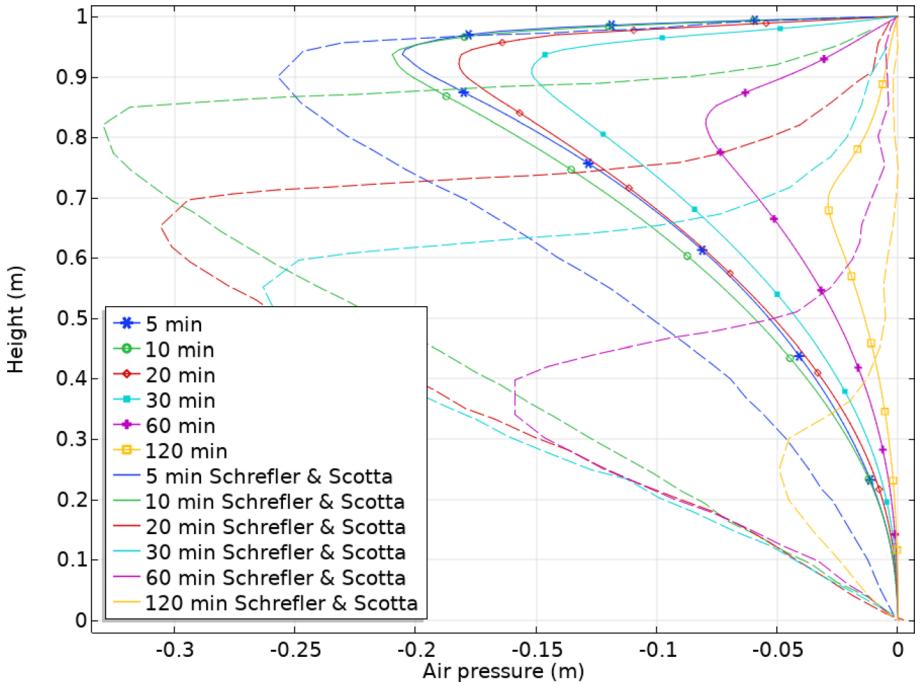

Fig. 4 Simulation results versus Schrefler and Scotta's results (air pressure)

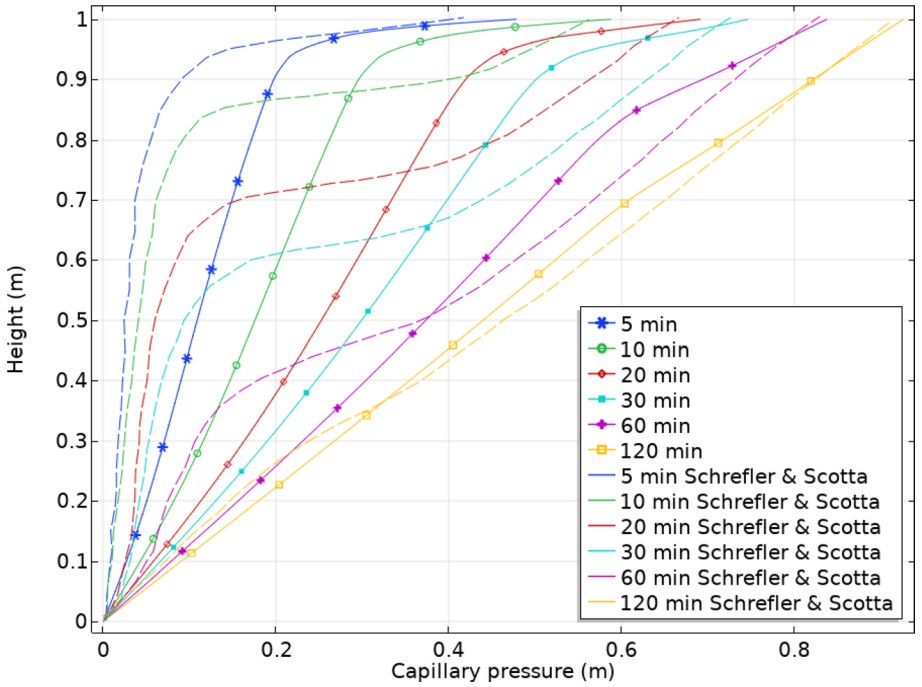

Fig. 5 Simulation results versus Schrefler and Scotta's results (capillary pressure)

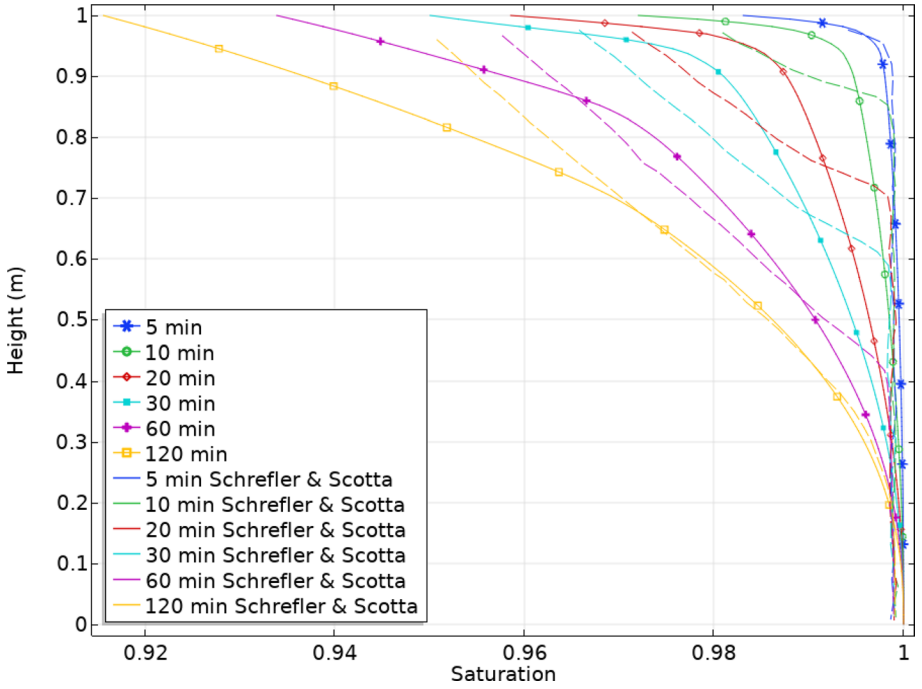

Fig. 6 Simulation results versus Schrefler and Scotta's results (water saturation)

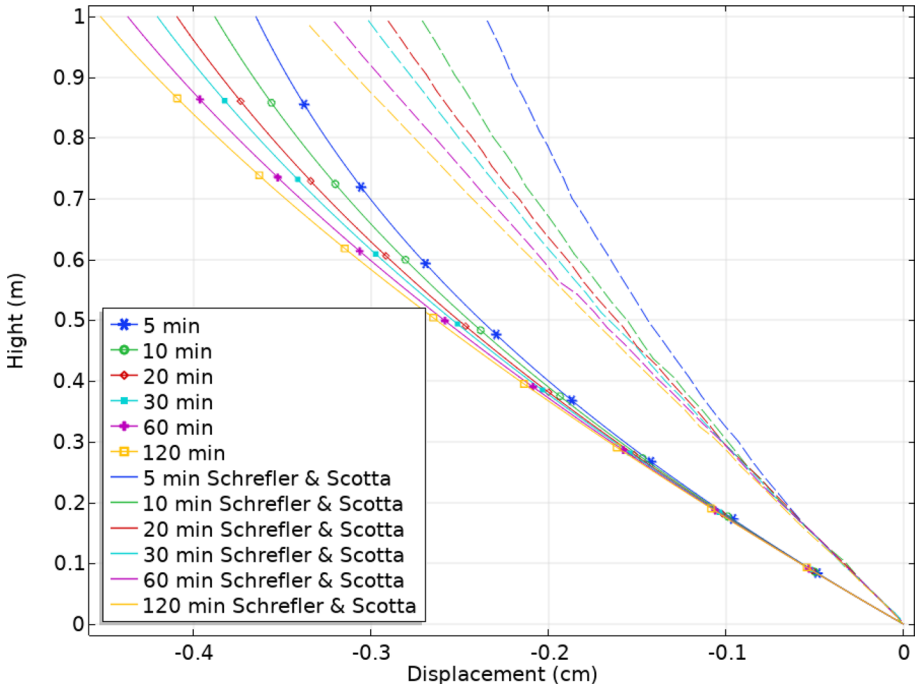

Fig. 7 Simulation results versus Schrefler and Scotta's results (displacement)

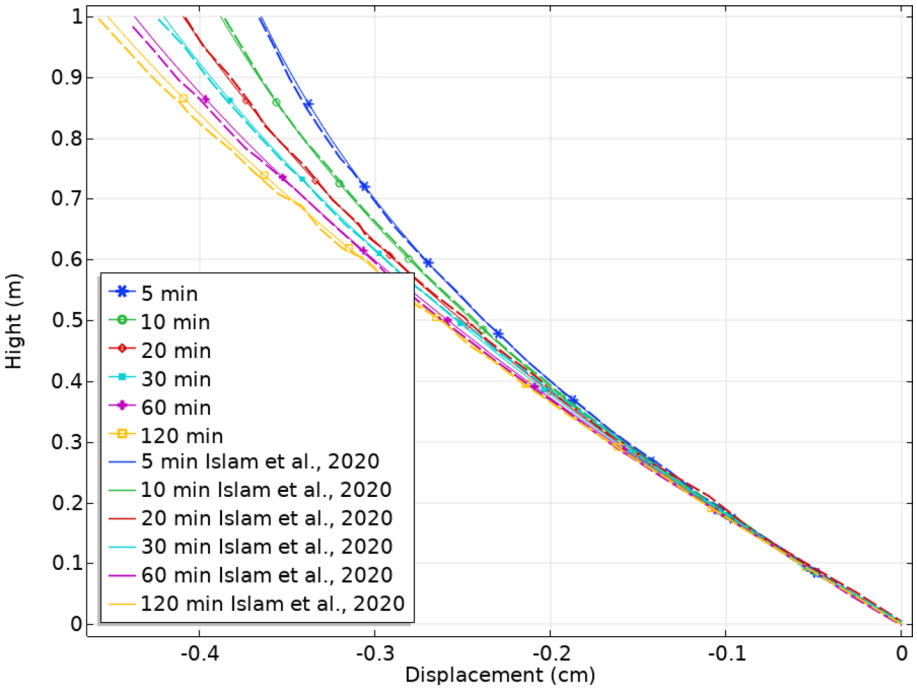

Fig. 8 Simulation results versus Islam et al. results (displacement)

3.2 Triaxial Pressure Device Experiment

Liakopoulos (1965) did not measure the gas pressure or flowrate in the conducted experiment; thus, another experiment is required to validate gas pressure/flowrate results. Popp et al. (2008) conducted a laboratory experiment using a triaxial pressure device with ultrasonic sensors to measure gas flow speed. Researchers such as Fall et al. (2014) used this experiment to validate their HM model. The model proposed in this research will be used to simulate the experiment and compared with the experiment results (Popp et al. 2008).

Laboratory experiments were performed on the Opalinus Clay specimen. The specimen was sampled from Mont Terri (Switzerland). Triaxial loading, strength, and gas injection tests were applied to the clay samples. The specimen was 150.45 mm in length with 73.59 mm in diameter. The acoustic velocities and gas permeability were measured parallel to the sample axis during the experiment. The top and the bottom of the specimen were drilled, and nitrogen gas was injected at control pressure in the central borehole from the bottom side of the sample. The gas flow rate at the upper outflow borehole was then measured using ultrasonic sensors. A hydrostatic loading with a constant confinement pressure was applied, and the gas (nitrogen) presser increased as a step function. A detailed description of the experiment and characteristics of the clay is given by Popp and Salzer (2007) and Popp et al. (2008)

A 2D model geometry is created in Comsol Multiphysics with extra-fine triangular mesh (as shown in Fig. 9) to simulate and validate the proposed HMG model using the

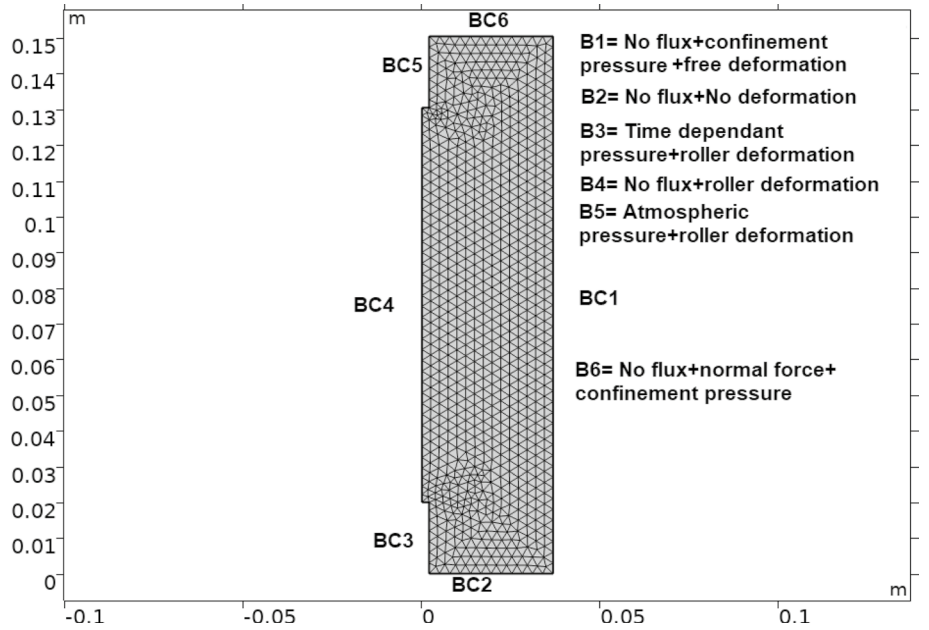

Fig. 9 2D triangular mesh geometry created and solved using Comsol Multiphysics

experiment. The figure shows the boundary condition as described in the original paper (Popp et al. 2008).

Figure 10 compares the gas flowrate experiment data and the simulation result of the proposed HMG model. During the experiment, the specimen started to crack (fails), which induced a noticeable increment in the permeability at 13,150 s.

The simulation result agrees with the experimental data in the elastic phase; however, since the proposed model is an elastic-model and deals only with constant permeability, the plastic deformation (crack) cannot be captured using such a model.

4 Conclusions

A fully coupled hydro-mechanical-gas (HMG) model based on the mixture coupling theory approach for water and gas flow was developed in this research. The coupled model is based on Helmholtz free energy equations and Biot's model. The model takes into consideration the coupled relation of solid deformation with the change in pressure. The change in water saturation and relative permeability is also considered since gas flow is included. The model was validated using Liakopoulos (1965) and Popp et al. (2008) experiment's data. The simulation results also compared to Schrefler and Scotta (2001) solution. The model was solved numerically using Comsol software (Finite element method software). The required parameters, Initial and boundary conditions were chosen from the available literature. The model showed good agreement with Liakopoulos' experimental data. The air pressure results showed slight differences from Schrefler and Scotta's results, which could be justified by some differences in the governing equations and the choice of solution

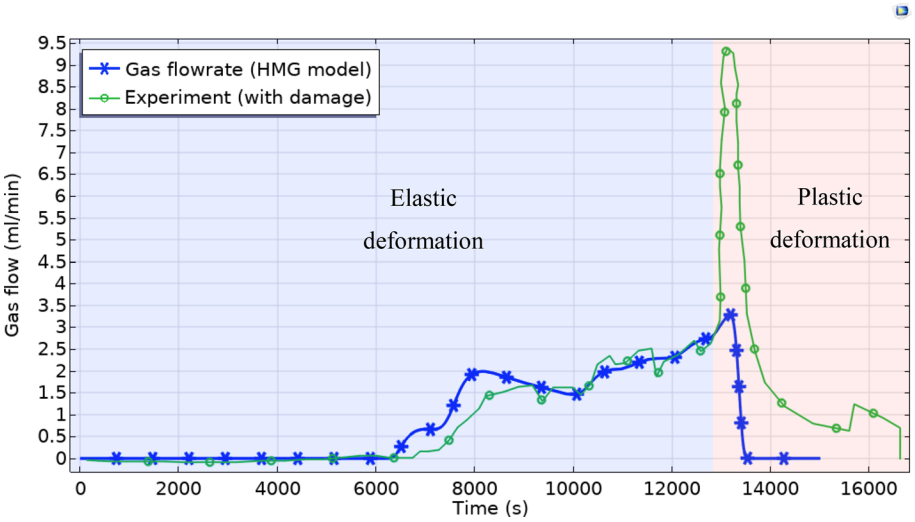

Fig. 10 Simulation results versus experimental data

algorithm. Since Liakopoulos (1965) did not measure the air pressure, Popp et al. (2008) triaxial experiment's data have been used to validate the gas behaviour part. The gas flowrate from the simulation showed a good agreement with the experimental data in the elastic phase. The model can be beneficial to many fields, particularly oil field studies as a CO2 injection simulation. This study offers opportunities for further future research. For example, this study could be extended by including a variable boundary condition to simulate a real case scenario, where the pressure and the porous media are not controlled at boundaries. Furthermore, more experiments on the flow of two-phase fluid in deformable porous media are required to measure and validate the air gas pressure and solid phase deformation behaviour.

Acknowledgements The authors would like to thank Kuwait Oil Company for its support and sponsoring this work; the second author would like to thank the CERES studentship support from school of civil engineering at the University of Leeds

Author contributions All authors contributed to the study conception and design. The first draft of the manuscript was written by Sulaiman Abdullah, and all authors commented on previous versions of the manuscript. All authors read and approved the final manuscript.

Funding Not applicable.

Declarations

Conflict of interest The authors have no relevant financial or non-financial interests to disclose. The authors have no conflicts of interest to declare that are relevant to the content of this article. All authors certify that they have no affiliations with or involvement in any organization or entity with any financial interest or non-financial interest in the subject matter or materials discussed in this manuscript. The authors have no financial or proprietary interests in any material discussed in this article.

Code Availability All data generated or analysed during this study are included in this published article.

Consent to Participate Not applicable.

Consent for Publication Not applicable.

Data Availability Not applicable.

Ethical Approval Not applicable.

References

Bandara, S., Ferrari, A., Laloui, L.: Modelling landslides in unsaturated slopes subjected to rainfall infiltration using material point method. Int. J. Numer. Anal. Meth. Geomech. **40**, 1358–1380 (2016)

Biot, M.A.: General theory of three-dimensional consolidation. J. Appl. Phys. **12**, 155–164 (1941)

Biot, M.A.: Theory of elasticity and consolidation for a porous anisotropic solid. J. Appl. Phys. **26**, 182–185 (1955)

Biot, M.A.: Mechanics of deformation and acoustic propagation in porous media. J. Appl. Phys. **33**, 1482–1498 (1962)

Biot, M.A., Temple, G.: Theory of finite deformations of porous solids. Indiana Univ. Math. J. **21**, 597–620 (1972)

Bowen, R.M.: Incompressible porous media models by use of the theory of mixtures. Int. J. Eng. Sci. **18**, 1129–1148 (1980)

Bowen, R.M.: Compressible porous media models by use of the theory of mixtures. Int. J. Eng. Sci. **20**, 697–735 (1982)

Brooks, R.H., Corey, A.T.: Properties of porous media affecting fluid flow. J. Irrig. Drain. Div. **92**, 61–88 (1966)

Cardoso, L., Fritton, S.P., Gailani, G., Benalla, M., Cowin, S.C.: Advances in assessment of bone porosity, permeability and interstitial fluid flow. J. Biomech. **46**, 253–265 (2013)

Chen, X., Hicks, M.A.: A constitutive model based on modified mixture theory for unsaturated rocks. Comput. Geotech. **38**, 925–933 (2011)

Fall, M., Nasir, O., Nguyen, T.: A coupled hydro-mechanical model for simulation of gas migration in host sedimentary rocks for nuclear waste repositories. Eng. Geol. **176**, 24–44 (2014)

Gawin, D., Simoni, L. & Schrefler, B.: Numerical model for hydro-mechanical behaviour in deformable porous media: a benchmark problem. In: Proceedings of the 9th International Conference on Computer Methods and Advances in Geomechanics, pp. 1143–1148. (1997)

Heidug, W., Wong, S.W.: Hydration swelling of water-absorbing rocks: a constitutive model. Int. J. Numer. Anal. Meth. Geomech. **20**, 403–430 (1996)

Hu, R., Chen, Y., Zhou, C.: Modeling of coupled deformation, water flow and gas transport in soil slopes subjected to rain infiltration. Sci. China Technol. Sci. **54**, 2561–2575 (2011)

Islam, M., Huerta, N., Dilmore, R.: Effect of Computational schemes on coupled flow and geo-mechanical modeling of CO2 leakage through a compromised well. Computation **8**, 98 (2020)

Katachalsky, A., Curran, P.F.: Nonequilibrium Thermodynamics in Biophysics. Harvard University Press, Cambridge, MA (1965)

Kim, Y.-S., Kim, J.: Coupled hydromechanical model of two-phase fluid flow in deformable porous media. Math. Probl. Eng. (2013)

Klika, V.: A guide through available mixture theories for applications. Crit. Rev. Solid State Mater. Sci. **39**, 154–174 (2014)

Krishnan, J.M., Rao, C.L.: Mechanics of air voids reduction of asphalt concrete using mixture theory. Int. J. Eng. Sci. **38**, 1331–1354 (2000)

Laloui, L., Klubertanz, G., Vulliet, L.: Solid–liquid–air coupling in multiphase porous media. Int. J. Numer. Anal. Meth. Geomech. **27**, 183–206 (2003)
Lewis, R.W., Schrefler, B.A.: The Finite Element Method in the Static and Dynamic Deformation and Consolidation of Porous Media. Wiley, New Jersey (1998)
Liakopoulos, A.: Transient Flow Through Unsaturated Porous Media [Ph. D. thesis]. University of California, Berkeley, Calif, USA (1965)
Maina, F.Z., Ackerer, P.: Ross scheme, Newton-Raphson iterative methods and time-stepping strategies for solving the mixed form of Richards' equation. Hydrol. Earth Syst. Sci. **21**, 2667–2683 (2017)
Milly, P.C.D.: Moisture and heat transport in hysteretic, inhomogeneous porous media: a matric head-based formulation and a numerical model. Water Resour. Res. **18**, 489–498 (1982)
Narasimhan, T.: The significance of the storage parameter in saturated-unsaturated groundwater flow. Water Resour. Res. **15**, 569–576 (1979)
Please, C., Pettet, G., McElwain, D.: A new approach to modelling the formation of necrotic regions in tumours. Appl. Math. Lett. **11**, 89–94 (1998)
Popp, T., Salzer, K.: Anisotropy of seismic and mechanical properties of Opalinus clay during triaxial deformation in a multi-anvil apparatus. Phys. Chem. Earth Parts a/b/c **32**, 879–888 (2007)
Popp, T., Salzer, K., Minkley, W.: Influence of bedding planes to EDZ-evolution and the coupled HM properties of Opalinus Clay. Phys. Chem. Earth Parts a/b/c **33**, S374–S387 (2008)
Schrefler, B.A., Scotta, R.: A fully coupled dynamic model for two-phase fluid flow in deformable porous media. Comput. Methods Appl. Mech. Eng. **190**, 3223–3246 (2001)
Schrefler, B.A., Xiaoyong, Z.: A fully coupled model for water flow and airflow in deformable porous media. Water Resour. Res. **29**, 155–167 (1993)
Siddique, J., Ahmed, A., Aziz, A., Khalique, C.: A review of mixture theory for deformable porous media and applications. Appl. Sci. **7**, 917 (2017)
Truesdell, C.: Sulle basi della termomeccanica. Rend. Lincei **22**, 33–38 (1957)
Truesdell, C., Toupin, R.: The Classical Field Theories. Principles of Classical Mechanics and FIELD THEORY/PRINZIPIEn der Klassischen Mechanik und Feldtheorie. Springer, New York (1960)
Van Genuchten, M.T.: A closed-form equation for predicting the hydraulic conductivity of unsaturated soils. Soil Sci. Soc. Am. J. **44**, 892–898 (1980)
Wei, H., Chen, J.-S., Beckwith, F., Baek, J.: A naturally stabilized semi-Lagrangian meshfree formulation for multiphase porous media with application to landslide modeling. J. Eng. Mech. **146**, 04020012 (2020)